The activity of cevo4-based catalysts for ammonia-scr: impact of surface cerium enrichment

Parnian Peyrovi, Sylvain Gillot, Jean-Philippe Dacquin, Pascal Granger, Christophe Dujardin, Sylvain Gillot

The activity of $CeVO_4$-Based Catalysts for Ammonia-SCR: Impact of surface cerium enrichment

Parnian Peyrovi, Sylvain Gillot, Jean-Philippe Dacquin, Pascal Granger, Christophe Dujardin*

Univ. Lille, CNRS, Centrale Lille, Univ. Artois, UMR 8181, UCCS - Unité de Catalyse et Chimie du Solide, 59000 Lille, France

Abstract

The ammonia-SCR catalytic activity of unsupported $CeVO_4$ with an excess of CeO_2 was investigated in standard and fast-SCR conditions. Solids were obtained from a hydrothermal synthesis route under a mild condition and then stabilized after aging in a wet atmosphere at 600 and 850°C. Particular attention was paid to the role of excess CeO_2 and the consequences of hydrothermal aging on physical-chemical properties and catalytic activity. The XRD patterns put into evidence the formation of the zircon-type structure of $CeVO_4$ in agreement with a segregation of cubic face-centered structure of ceria (CeO_2). Along with adding an excess of CeO_2, high specific surface area (102 m^2/g) for the 11wt.% CeO_2 /$CeVO_4$ solid was obtained. The presence of CeO_2 nanoparticles in addition to $CeVO_4$ nanoparticles have limited the decrease in the specific surface area after aging at 600 and 850°C. The catalyst with 11wt.% CeO_2 /$CeVO_4$ exhibited the best catalytic performances in standard and fast SCR conditions after thermal aging at 600°C.

Keywords: ammonia-SCR, nitrogen oxides, nitrous oxide, vanadium, $CeVO_4$

Running head: Activity of $CeVO_4$-Based Catalysts for NH_3-SCR: Impact of cerium enrichment

*Christophe Dujardin, christophe.dujardin@centralelille.fr

1 Introduction

Nitrogen oxides (NO_x) emitted from diesel engines are harmful to human health and environment. SCR of NO_x with NH_3 is considered to be the most efficient technology for reducing NO_x emission in the presence of excess oxygen [1]. However, even though this technology has been available for decades for stationary sources, the improvement of the operating temperature window and hydrothermal stability of the SCR catalysts is a big challenge to meet the emission standards of NO_x from-mobile sources. Complex systems for the simultaneous treatment of NO_x, hydrocarbon, and soot have been introduced, which are generally expensive and can lead to the reduction of engine efficiency [2, 3]. The engine space limitation has forced manufacturers to seek an alternative solution with the combination of different aftertreatment components. The incorporation of SCR catalyst directly into the porosity of the diesel particle filter (DPF) would save space, money and simplify the post-processing vehicles equipped with a diesel engine. Such implementation requires improved thermal resistance of the SCR catalyst due to the exotherms related to the periodic regeneration of DPF [4]. Existing urea SCR active catalysts can serve as a starting point for a catalyst that is both active and stable under these new conditions. Important parameters influencing the activity of a catalyst are defined mainly by acidity and redox power [5]. Therefore, deactivation of the catalysts is synonymous to degradation of their acid and/or redox properties, in particular when they are dealing with high temperature in the presence of water [6]. The aim of this study is focused on the development of new thermally stable active phases which are capable of maintaining their catalytic performances after hydrothermal aging at high temperature.

The current benchmark catalyst used for the aftertreatment of stationary sources is V_2O_5-WO_3/TiO_2 which is highly active for NH_3-SCR especially in standard SCR condition. The SCR catalyst mostly includes anatase TiO_2 as support material, WO_3 as promoter of activity and stability and V_2O_5 as the active redox species [7]. The mechanism of NH_3-SCR over vanadia-containing catalysts reported in the literature usually assumes that acidic sites are needed for facilitating ammonia adsorption [8, 9].

There are still some problems with the utilization of this catalyst, such as a limited operating temperature window and low N_2 selectivity at high temperature which reduce its further application in the deNO_x process for mobile sources [10]. The main drawback is associated to the toxicity of V_2O_5 oxide and its volatilization above the sublimation temperature (670°C) [11].

Among the wide variety of catalysts tested in recent years, those based on modified ceria attract considerable attention in NH_3-SCR [12, 13]. Due to its textural properties and ability to interact with other components, cerium oxide can be used as the promoter [14], support [15] and active phase [16] in NH_3-SCR.

Ceria is considered as a very active oxide in the SCR reaction, owing to its considerable oxygen storage capacity [17], facility of changing oxidation state between Ce^{4+} and Ce^{3+} [18] and its reactivity in enhancing the oxidation of NO to NO_2 [19, 20]. Moreover, ceria-based NH_3-SCR catalysts have attracted much attention due to their non-toxic and relatively cheap characteristics [21, 22, 23]. In spite of that, there are still large numbers of problems, such as its sulfur resisting capacity [24, 25] aging resistance [26] and low selectivity to N_2 [27] still to be solved. Hydrothermal aging of the catalyst is well known as a negative impact on catalytic activity that significantly decreases the NO_x conversion capability of an SCR system [28, 29]. However, limited information is available in the literature with regards to the effect of hydrothermal aging on NH_3-SCR NO_x conversion of CeO_2 -modified catalysts [26, 30]. $CeVO_4$ -based materials have received recent attention in view of their potential applications in NH_3-SCR [31, 32, 33]. Gillot et al. underlined the potential of unsupported $CeVO_4$ solid prepared by the hydrothermal method in NH_3-SCR reaction. They showed that the solid is predominantly composed of tetragonal $CeVO_4$ phase but a slight segregation of cubic CeO_2 phase is also put into evidence [34].

The present study is devoted to the role of CeO_2 in the catalytic activity of $CeVO_4$ in the NH_3-SCR reaction. The segregation of CeO_2 during the synthesis will be investigated through physicochemical characterization. It will show that excess CeO_2 in the catalyst formulation leads to improved catalytic activity after aging at 600 and 850°C.

2 Experimental

2.1 Catalyst Preparation and Physicochemical Characterization

The samples were prepared by hydrothermal method. Appropriate amounts of vanadium salt Na_3VO_4 (99.98 wt.% Sigma-Aldrich) were dissolved in 50mL of distilled water at room temperature. The solution was acidified to a pH value close to 1.8 with the nitric acid solution at room temperature. The excess of $Ce(NO_3)_3 \cdot 6H_2O$ was added to the vanadium solution under stirring. Sodium hydroxide solution (1M) was added dropwise into the above solution to adjust the pH to 7. pH values during precipitation decrease sharply, that can be explained by the following set of Equations (1) – (2) hence leading to the formation of $CeVO_4$.

$$VO_2^+ + 2OH^- = VO_4^{3-} + 2H^+ \quad (1)$$

$$Ce^{3+} + VO_4^{3-} = CeVO_4 \quad (2)$$

The resulting mixture suspension was transferred into a 50 ml Teflon-lined stainless-steel autoclave and sealed tightly. Hydrothermal synthesis was carried out at 180°C for 24 h in an oven without shaking or stirring. After cooling to room temperature, the precipitates were collected, washed with distilled water and absolute ethanol several times, and then dried in air at 80°C for 24 h.

Chemical composition was determined using inductively coupled plasma atomic emission spectroscopy (ICP-OES) Varian Vista Pro. A charge-coupled device (CCD) covering a broad spectral range (from 167 to 765 nm) was used as a detector.

Specific surface area of mixed oxides was measured by adsorption of N_2 according to BET method. The specific areas were determined using a FlowSorb III apparatus (Micromeritics) equipment after heating under vacuum at 100°C for 45 minutes to remove adsorbed residual impurities.

All the samples were characterized by powder X-ray diffraction (XRD) on a D8 Advance Bruker X-ray diffractometer. XRD patterns were recorded from 5 to 80° (2θ) with a scanning step of 0.02° and an acquisition time of 0.5s.

The surface composition of samples over a thickness between 5 and 10 nm was determined by X-Ray Photoelectron Spectroscopy (XPS). XPS measurements were carried out using an AXIS Ultra DLD Kratos spectrometer. The system includes a monochromatic X-ray source and an Al-Mg double anode. A spectral decomposition of the experimental photopeaks was analyzed using the CasaXPS software.

Temperature-programmed reduction with hydrogen (H_2-TPR) of the catalysts was performed in Micromeritics Autochem 2920 equipment, and with a temperature ramp from 20 to 1000°C (10°C/min) under 5% H_2/Ar.

Raman spectra were acquired using a confocal Raman microscope (Xplora, Horiba Jobin Yvon). The 532 nm diode laser was used to excite the sample through a 100X objective. The Raman signal collected in the backscattering mode was dispersed in the built-in spectrograph by a 1200 gr/mm grating and detected by an Open-Electrode CCD.

2.2 Catalytic measurements

Catalytic performances were evaluated on catalyst powder (150–300 μm, 80 mg) in 1 g SiC (210 μm) in a plug-flow reactor. The catalytic performances were estimated in two reaction mixtures corresponding to the NO/NO_x molar ratios =1/2 and 1 (with NO_x = NH_3 = 400ppm, 10% CO_2, 10% H_2O and 8% O_2 diluted in He) from 200°C to 500°C with a heating rate of 5°C/min (GHSV = 250 000 $mL.h^{-1}.g^{-1}$). Before the activity test, the catalyst was aged at 600 or 850°C for 5 hours in the wet atmosphere (10% H_2O in air) with an hourly space velocity (GHSV) of 42000$mL.h^{-1}.g^{-1}$. The outlet gas concentration (N_2 and N_2O) was analyzed during NH_3-SCR with a μGC equipped with two distinct columns (molecular sieve 5Å and porapak Q). The NO_x conversion is calculated from the N_2 and N_2O concentrations according to Equation (3) and N_2O selectivity determined from Equation (4):

$$X_{N_2O+N_2} = \frac{2 * (C_{N_2} + C_{N_2O})}{C_{NO_x\,initial}} * 100 \qquad (3)$$

$$S_{N_2O} = \frac{C_{N_2O}}{(C_{N_2} + C_{N_2O})} * 100 \qquad (4)$$

3 Results and Discussion

The series of $CeVO_4$ catalysts were synthesized through the hydrothermal method. As a general trend, the vanadium sub-stoichiometry associated with V/Ce = 0.83 and 0.81 is in agreement with the segregation of the corresponding Ce content. It corresponds to 11 wt.% and 13 wt.% CeO_2 respectively (Table 1). The series of $CeVO_4$ catalysts with 0, 11 and 13 wt.% CeO_2 in excess will be noted as Ce-CeV, 11Ce-CeV and 13Ce-CeV respectively.

3.1 Catalytic activity of Ce-CeV samples

The NO_x conversion for different NO/NO_x ratio on Ce-CeV, 11Ce-CeV, and 13Ce-CeV catalysts after an ex-situ hydrothermal aging at 600°C or 850°C was investigated. NO_x concentration in diesel exhaust is usually composed of more than 90% NO [35]. On one hand, the main reaction of SCR with ammonia with NO/NO_x ratio equal to 1 so-called standard SCR will be:

$$2NO + 2NH_3 + 1/2O_2 \rightarrow 2N_2 + 3H_2O \qquad (5)$$

On the other hand, the NO_x conversion with equimolar amounts of NO and NO_2 (NO/NO_x=0.5) so-called fast-SCR has a higher reaction rate than that of standard SCR and is the following:

$$NO + NO_2 + 2NH_3 \rightarrow 2N_2 + 3H_2O \qquad (6)$$

Fast-SCR reaction is usually proposed as a practical possibility to increase the performance of diesel engine $DeNO_x$ system [36, 37].

Standard SCR

The NO_x conversion during standard-SCR condition versus temperature is collected in Fig. 1A on the Ce-CeV catalysts aged in the presence of steam in air at 600°C. All catalysts possess high N_2 selectivity (100%) in the whole temperature range. The NO_x conversion increases on the reference Ce-CeV catalyst from 30% conversion at 200°C to a maximum NO_x conversion of 50% at 400°C. The NO_x conversion declines when the temperature rises to 400°C on Ce-CeV catalyst due to the oxidation

of NH_3 with oxygen. The NO_x conversion decreases to 35% at 500°C due to the competitive oxidation of NH_3 with oxygen that leads to lower NO_x conversion. Interestingly, significant changes in NO_x conversion are observable with regards to the amount of CeO_2 in excess. 11Ce-CeV catalyst has a much higher NO_x conversion between 200 and 450°C. The remarkable promotion effect of CeO_2 with the doping amount of 11% in standard-SCR condition is observed at medium temperature with a maximum conversion of 80% between 300–350°C. However, a NO_x conversion drop can be detected at 500°C which can be due to the strengthening of the competitive oxidation of NH_3 at high temperature. 13Ce-CeV catalyst has a lower NO_x conversion capability with a maximum NO_x conversion of 45% at 300°C. The undesirable ammonia oxidation by oxygen is the predominant side reaction that results in decreasing NO_x conversion above 350°C [38;39].

Fast SCR

Under Fast-SCR conditions, an equimolar mixture of NO and NO_2 is introduced into the reactor (Fig 1.B). Catalytic measurements in fast SCR conditions on Ce-CeV solid lead to a higher NO_x conversion of approximately 89 % versus 36 % for respectively fast and standard SCR conditions at 250°C. Kobel et al. [40] found that the reaction involving an equimolar NO and NO_2 feed mixture (fast-SCR) is significantly faster than the standard-SCR reaction. They reported in fast-SCR condition that gaseous NO_2 replaces oxygen as a more effective oxidizing agent, hence allowing faster reoxidation of the vanadium sites. Topsoe et al. suggested that the rate determining step in NH_3-SCR reaction over vanadium-containing catalysts is reoxidation of V^{4+}–OH to V^{5+}=O species [41]. On the other hand, the conversion curves converge at high temperature irrespective of the operating conditions.

NO_x conversion increases from 65% at 200°C to a maximum of 89% at 250°C on Ce-CeV catalyst and then starts to decrease. The NO_x conversion decreases from 80% to 30% between 300 and 500°C. The addition of CeO_2 on 11Ce-CeV leads to an increase of NO_x conversion between 250–400°C, with maximum NO_x conversion of 95% at 250°C. The NO_x conversion of 11Ce-CeV catalyst is much higher than that of the reference Ce-CeV catalyst, but its NO_x conversion is quite limited in the low

(<250°C) and in the high (>450°C) temperature range. Further addition of CeO_2 on 13Ce-CeV has a detrimental effect on NO_x conversion, which doesn't exceed 60% in the whole temperature range.

Ce-CeV catalyst is 100% selective towards N_2 (200–450°C) in fast SCR whereas at 500°C the N_2 selectivity declines to 90%. The 11Ce-CeV catalyst has the highest N_2 selectivity among the investigated catalysts in fast SCR. Moreover, a lower N_2 selectivity of 13Ce-CeV can be observed suggesting that the oxidative function on the 13Ce-CeV catalyst promote the non-selective oxidation of NH_3 at the expense of NH_3-SCR.

Impact of thermal aging

The NO_x conversion in fast-SCR condition versus temperature is reported for the catalysts aged at 850°C in Fig. 1C. It is obvious that hydrothermal aging at 850°C results in the decrease of NO_x conversion, which might be due to the sintering of active components. The NO_x conversion reaches 15% at 200°C on Ce-CeV catalyst, a maximum of 40% is recorded at 300°C and NO_x conversion decreases to 5% at 500°C. The NO_x conversions of catalysts with excess of cerium remain below 40% underlining the detrimental effect of thermal aging at 850°C. The NO_x conversion of 35–39% on 13Ce-CeV catalyst is significantly enhanced in a wide range of temperature (250–450°C). Further temperature increase results in a lower NO_x conversion (25% at 500°C). The 13Ce-CeV catalyst has the higher NO_x conversion in fast-SCR compared to the reference Ce-CeV and 11Ce-CeV catalysts but a lower selectivity towards nitrogen formation, all selectivities decrease monotonically as a function of the temperature. The N_2O selectivity of the 13Ce-CeV catalyst increases noticeably at 300–350°C with quite a large amount of N_2O being finally formed. The amount of CeO_2 in excess has limited impact on NO_x conversion in standard SCR when the catalysts are aged at 850°C (Fig. S1).

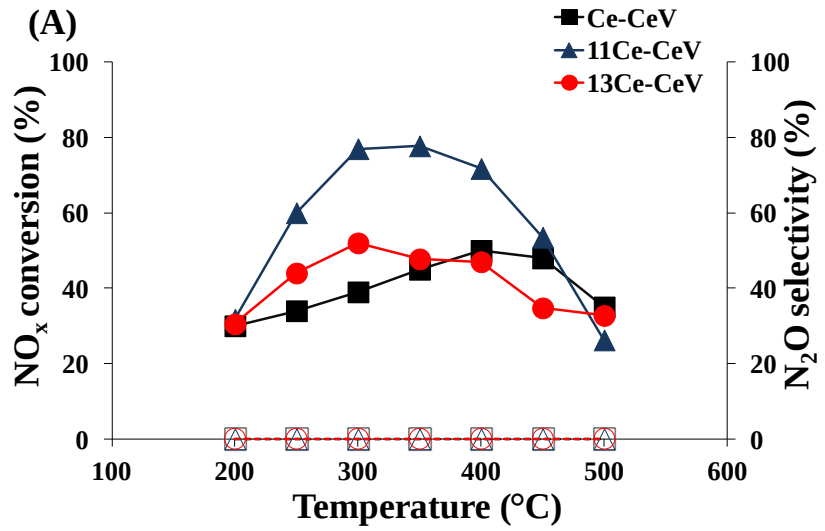
(A)
Ce-CeV
11Ce-CeV
13Ce-CeV
NOx conversion (%)
N2O selectivity (%)
Temperature (°C)
100
200
300
400
500
600
0
20
40
60
80
100

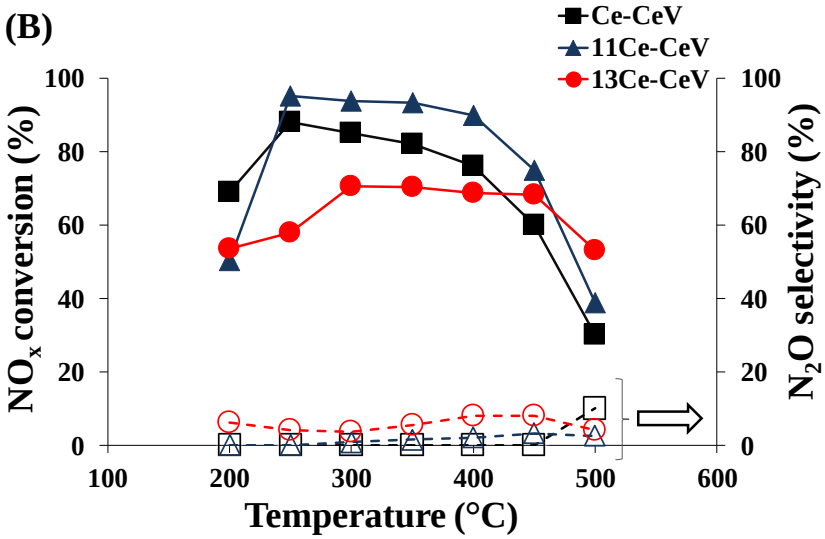
(B)
Ce-CeV
11Ce-CeV
13Ce-CeV
NOx conversion (%)
N2O selectivity (%)
Temperature (°C)
100
200
300
400
500
600
0
20
40
60
80
100

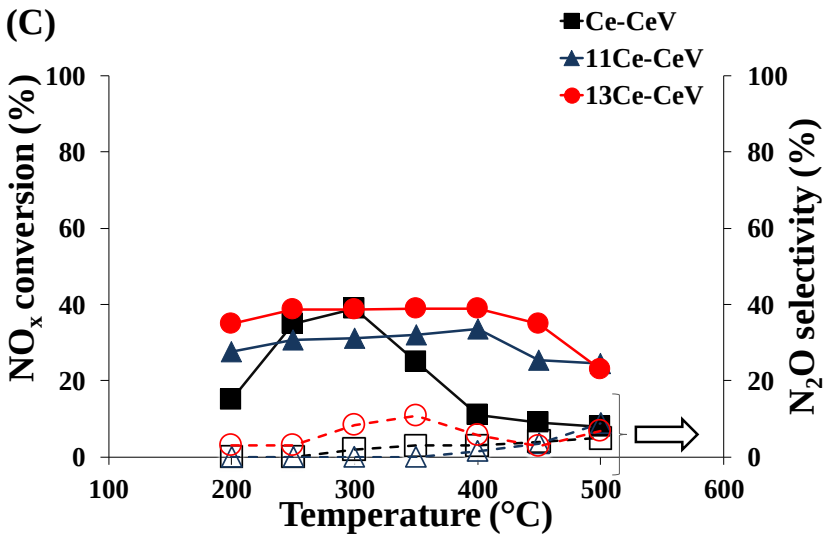

Fig. 1 NO_x conversion (solid lines) and N_2O selectivity (dotted line) during the standard-SCR (A) and fast-SCR (B) reaction after aging at 600°C; fast-SCR (C) after aging at 850°C

3.2 Characterization of Bulk and Surface properties

3.2.1 Bulk Properties

The powder diffractograms recorded for the catalysts obtained after aging at 600 and 850°C in a wet atmosphere are compared in Fig. 2. The tetragonal zircon structure of $CeVO_4$ is detected for all catalysts with characteristic lines located at 2θ = 18, 24, 32 and 48°. Additional X-ray diffraction lines appear at 2θ = 28.5, 33 and 47.5° and are ascribed to the face-centered fluorite structure of CeO_2 on all Ce-CeV samples aged at 600°C. The formation of ceria could be explained by the dehydration of $Ce(OH)_3$ during the hydrothermal synthesis and following oxidation with air into CeO_2 [42].

Table 1 lists the crystallite sizes that have been estimated using the Scherrer equation from reflections corresponding to the (200) plane of $CeVO_4$ and (111) planes of CeO_2 at 2θ = 24° and 28.5° respectively. The fresh solids generally have a $CeVO_4$ crystallite diameter from 15 to 27 nm.

The specific surface area is also presented in Table 1. The high specific surface areas between 46 to 102 m^2/g on fresh solids can be explained by the relatively low temperature (180°C) during the hydrothermal synthesis. These values are in agreement with the crystallite diameter evolution.

Impact of thermal aging

Hydrothermal aging at 850°C leads to crystallographic changes mainly associated to the appearance of a phase assigned to rhombohedric Ce_7O_{12} for all catalysts except for the catalyst with the lower Ce loading (Ce-CeV solid) (Fig. 2B). The segregation of Ce_7O_{12} phase is not necessarily useful in NH_3-SCR since Ce_7O_{12} oxide possesses pairs of anionic oxygen vacancies on the axis [43]. The catalysts with cerium in excess have smaller crystallite size in comparison to the reference Ce-CeV after aging at 600°C. Along with increasing the excess of cerium from 11 to 13 wt.% CeO_2, the crystallite diameter increases (44 to 61 nm). The comparison of crystallite diameter after aging at 600 and 850°C illustrates the higher sensitivity of $CeVO_4$ than CeO_2 phase to sintering. By increasing cerium content on Ce-CeV solid, the CeO_2 phase is slightly less sensitive to sintering in comparison to the other phase.

The theoretical values of the specific surface area (S_{th}) calculated from the crystallites' diameter of $CeVO_4$ obtained by XRD analysis are presented in Table 1. The comparison of experimental and theoretical values (S_{exp} and S_{th} respectively) can be used to distinguish if the sintering process is driven either by agglomeration and/or crystal growth phenomena. It should be noticed that a good agreement is obtained with S_{th}/S_{exp} close to 1 for the fresh catalysts. The addition of 11 wt.% CeO_2 increases the specific surface area of the fresh catalyst. After aging at 600°C, a beneficial effect of CeO_2 addition is clearly observed, the modified solids with 11 wt.% of CeO_2 in excess preserving a specific surface area approximately five times higher than that of the Ce-CeV reference solid. The presence of CeO_2 nanoparticles can limit the $CeVO_4$ sintering by acting as a diluent for $CeVO_4$ nanoparticles thus limiting the loss of specific surface area. Indeed, an aging temperature of 850°C decreases the specific surface area of all solids. However, the S_{th}/S_{exp} values increase after aging at 850°C suggesting that the

loss of specific surface area is a combination of both crystal growth and agglomeration processes for all solids.

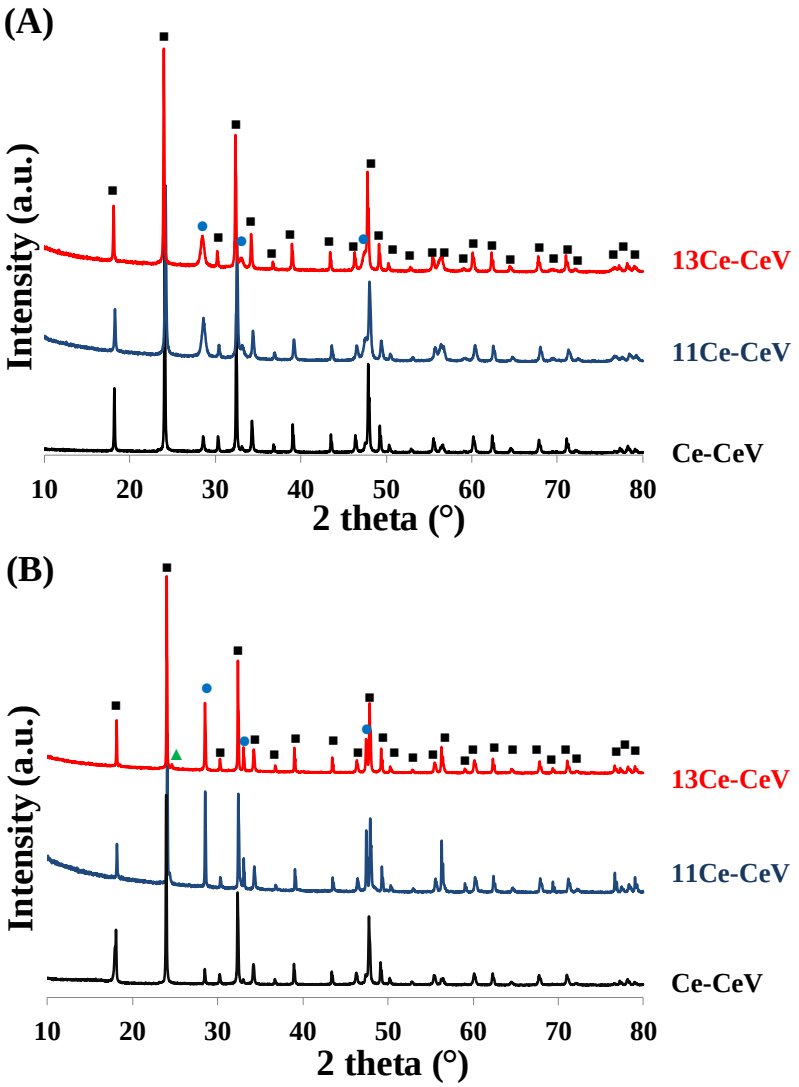

Fig. 2 XRD patterns recorded on catalysts aged at 600°C (A) and aged at 850°C (B)—(■) tetragonal phase of $CeVO_4$, (●) cubic structure of CeO_2 (▲) rhombohedric phase of Ce_7O_{12}

The redox property of catalysts is involved in the catalytic cycle of NH_3-SCR reactions and is investigated through H_2-temperature-programmed reduction. Two peaks are clearly observed in the whole reduction process as shown in Fig. 3 for the series of Ce-CeV catalysts. The peak above 700°C is associated to the reduction of $CeV^{+5}O_4 \rightarrow CeV^{+3}O_3$ [44]. The maximum of this peak shifts to lower temperature (from 786 to 770°C) with the increase of CeO_2 loading, implying that the 11Ce-CeV and 13Ce-CeV catalysts have better redox properties than that of Ce-CeV catalyst. The less intense reduction peak observed at low temperature could either reflect the reduction of surface Ce^{4+} species

to Ce^{3+} both in CeO_2 or the reduction of V^{5+} of the vanadate groups, which is difficult to be distinguished due to the similar reduction temperature [45]. This reduction peak shifts to the higher temperature by increasing CeO_2 loading whereas the H_2 consumption progressively increases from 0.07 to 0.12 mmol H_2/g. The quantity of reducible V^{5+} species of the Ce-CeV catalyst is very weak. The evolution of vanadate concentration at the surface can be related to the change of NO_x conversion and the N_2 selectivity. The catalyst with 11 wt.% of cerium in excess (11Ce-CeV) causes the exposure of more vanadium species on the surface, thus promoting the NH_3-SCR reactions performances. However, when the amount of Ce increases to 13wt.%, the quantity of extra surface vanadium species on CeO_2 and/or $CeVO_4$ increases which causes the promotion of the unexpected NH_3 oxidation and hence decrease both the NO conversion as well as the N_2 selectivity [20].

Fig. 4 compares the Raman spectrum of solids after aging at 600°C. Strong Raman lines at 771 and 840 cm^{-1} correspond to the anti-symmetric (B_{1g}) and symmetric (A_{1g}) stretching of VO_4^{3-} tetrahedrons. The bending modes of B_{1g} and A_{1g} are detected at 443 and 367 cm^{-1}, respectively. The Raman line at 258 cm^{-1} is characteristic of the B_{2g} bending mode of the VO_4^{3-} tetrahedrons. The external mode of $CeVO_4$ vibration appears at 214 cm^{-1}. It should be noted that the characteristic Raman lines of V_2O_5 are not detected for the series of Ce-CeV solids. The proximity of the CeO_2 line (F_{2g} mode to ~460 cm^{-1}) and the combination line $E_g + B_{2g}$ of VO_4^{3-} at 443 cm^{-1} (corresponding to $CeVO_4$) prevents a clear identification of the CeO_2 phase by Raman spectroscopy [20, 46].

The ratio between Raman lines at ~450 cm^{-1} and at 367 cm^{-1} reflect the presence of segregated CeO_2 in the solid. The ratio is maximal for the 11Ce-CeV solid. Additional EDX analysis performed on Ce-CeV solid aged at high temperature (Fig. S2 and S3) underlines the presence of small particles of CeO_2 in addition to $CeVO_4$ and the fact that the cerium concentration (Table S1) can significantly vary depending on the analysed particle.

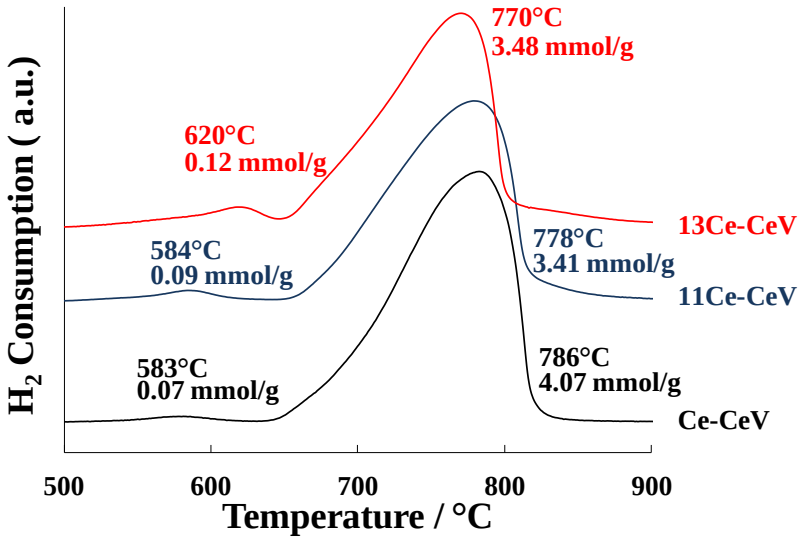

Fig. 3 H_2 consumption during H_2-temperature-programmed reduction profiles on Ce-CeV catalysts aged at 600°C

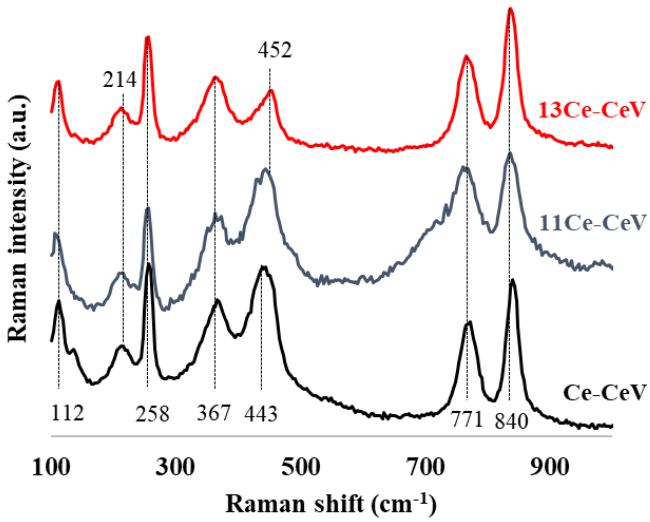

Fig. 4 Comparison of Raman spectra of Ce-CeV catalysts aged at 600°C

Table 1 Physicochemical properties of solids prepared via the hydrothermal method and aged at 600 and 850°C in Air + 10 %H_2O

Catalysts	Thermal treatment	Bulk atomic ratio V/Ce[a]	Na content[a] wt.%	Crystallite size (nm)[b]		SSA (m^2 g^{-1})		S_{th}/S_{exp}
				$CeVO_4$	CeO_2	Experimental	Theoretical[c]	
Ce-CeV	Unaged	0.94	0.50	27	46	46	47	1.0
	Aged 600°C	0.94		85	57	6	15	2.5
	Aged 850°C	1.20		96	82	0.5	13	26
11Ce-CeV	Unaged	0.83	0.42	15	8	102	80	0.7
	Aged 600°C	0.83		44	20	32	29	0.9
	Aged 850°C	1.10		81	71	3	15	5.0
13Ce-CeV	Unaged	0.81	0.07	21	9	60	60	1.0
	Aged 600°C	0.81		61	19	20	20	1.0
	Aged 850°C	1.06		77	68	2.5	16	6.4

[a] From ICP-OES analysis

[b] From XRD analysis

[c] Calculated from the crystallite size of $CeVO_4$ obtained from XRD with $S_{th} = 6/ (\rho.d_{crystallite})$

The oxidation state and the surface atomic concentrations of cerium, vanadium, and oxygen are investigated through the characterization of Ce 3d, O 1s and V 2p core levels (Fig. S4, S5). Results are summarized in Table 2. The Ce 3d spectra are complex and can be deconvoluted into $3d_{5/2}$ and $3d_{3/2}$ spin-orbit components (labeled as v and u, respectively) describing the $Ce^{4+}\leftrightarrow Ce^{3+}$ electronic transitions (Fig. 5). The peaks v^0, v', u^0, and u' are characteristic of Ce^{3+} that are indicative of the $3d^{10}4f^1$ initial electronic configuration while v, v", v"', u, u", and u"' are attributed to Ce^{4+}, representative of the $3d^{10}4f^0$ electronic configuration. The four intense components v (BE ~ 882.5 eV), u (BE ~ 900.9 eV), v"' (BE ~ 898.2 eV), u"' (BE ~ 917.1 eV) as well as the two weaker components v" (BE ~ 889.4 eV) and u" (BE ~ 908.2 eV) are assigned to Ce^{4+} cations. The four other intense

components v' (BE ~ 885.6 eV), u' (BE ~ 903.7 eV), v^0 (BE ~ 881.3 eV) and u^0 (BE ~ 899.0 eV) that are overlapped by v''' and u' components corresponds to Ce^{3+} [47, 48]. Hence both Ce^{3+} and Ce^{4+} cations coexist in the series of Ce-CeV catalysts (Fig. S4). The evolution of Ce^{4+}/Ce^{3+} surface atomic ratio is reported in Table 2. The Ce^{4+}/Ce^{3+} ratio increases by adding CeO_2 and by aging at 600°C. After aging at 850°C, Ce^{4+}/Ce^{3+} ratio increases for Ce-13CeV and this ratio decreases for Ce-CeV and 11Ce-CeV solids. The O 1s photopeak is characterized by two contributions at 530.5 eV and 532.0 eV (Fig. S5) referring to the distribution at the surface of lattice oxygen O^{2-} (O_β) and adsorbed oxygen species (O_α) that are O_2^-, O^- or OH groups. It is widely accepted that O_α species are more active than O_β species due to their higher mobility [49], surface oxygen vacancies and defect sites [50]. In addition, O_α species enhance the fast-SCR reaction (equation 6) owing to the prior oxidation of NO to NO_2 [5]. The O_α/O_β ratio in Ce-CeV reference sample is calculated as 0.34 while that of Ce-11CeV and Ce-13CeV solids increase up to 0.49 and 0.41, respectively. These results suggest that a high activity for NO oxidation to NO_2 can enhance the fast-SCR activity towards low temperature with the high concentration of chemisorbed oxygen species. For the V 2p photopeak, the binding energy separation between the core levels V $2p_{1/2}$ (524.9 eV) and V $2p_{3/2}$ (517.6 eV) is 7.3 eV, corresponding to the oxidation states of V^{5+} [51]. The binding energies for the photopic V $2p_{3/2}$ remain almost unchanged for the series whatever the amount of CeO_2 or the hydrothermal aging. The estimates of V/Ce, V/O and Ce/O surface atomic ratio is presented in Table 2. The evolution of V/Ce surface atomic ratio reveals an increase in vanadium surface concentration after aging, especially at 850°C except for Ce-CeV catalyst. The Ce/O and V/O surface atomic ratios vary slightly with aging.

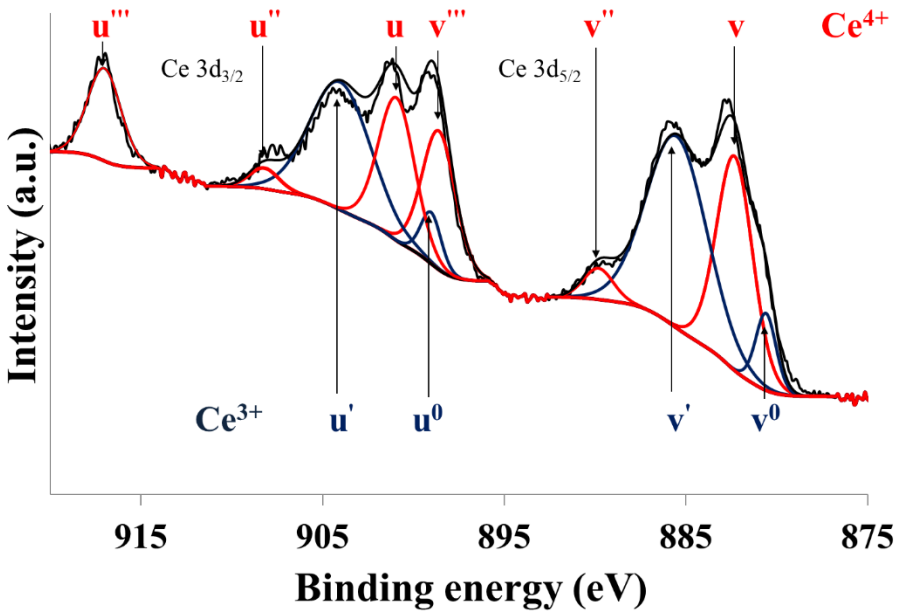

Fig. 5 Deconvolution of the Ce 3d core level on 11Ce-CeV catalyst after thermal aging at 600°C

Table 2 XPS analysis of samples aged at 600 and 850°C for 5 h in air and 10 vol. % H_2O

Catalyst	Thermal treatment	B.E. (eV)		Surface atomic ratio				
		$Ce3d_{5/2}$	$V2p_{3/2}$	Ce/O	V/O	V/Ce	Ce^{4+}/Ce^{3+}	O_α/O_β
Ce-CeV	Unaged	883.7	517.6	0.31	0.24	0.78	0.12	0.34
	Aged 600°C	883.5	517.7	0.26	0.25	0.94	0.23	0.27
	Aged 850°C	883.4	517.7	0.29	0.24	0.82	0.12	0.33
11Ce-CeV	Unaged	883.3	517.5	0.26	0.20	0.77	1.05	0.49
	Aged 600°C	883.2	517.6	0.25	0.20	0.83	1.35	0.57
	Aged 850°C	883.1	517.6	0.18	0.18	1.00	0.83	0.69
13Ce-CeV	Unaged	883.4	517.4	0.30	0.20	0.67	1.00	0.41
	Aged 600°C	883.3	517.4	0.30	0.22	0.73	1.00	0.30
	Aged 850°C	883.1	517.5	0.23	0.20	0.85	1.20	0.52

3.3 General Discussion

A series of $CeVO_4$ with an excess of CeO_2 (11 and 13 wt %) was synthesized by hydrothermal synthesis. The solids were aged ex-situ at 600 and 850°C in 10% H_2O in the air. The zircon-type structure of $CeVO_4$ is obtained after hydrothermal synthesis without additional calcination step and preserved after aging. The presence of segregated ceria revealed in XRD pattern and by SEM-EDX analysis is in agreement with the surface Ce^{4+} enrichment (XPS) that confirms the presence of CeO_2 at the surface of the catalyst. A greater sensibility of $CeVO_4$ phase towards sintering is put into evidence from the evolution of the specific surface area and XRD measurements after thermal aging. In fact, the thermal sintering of CeO_2 is more visible after aging at 850°C. As a matter of fact, the lower specific surface area and the larger crystallite size of Ce-CeV compared to 11Ce-CeV and 13Ce-CeV can be partly explained by the presence of CeO_2. The coexistence of two different crystalline phases with different crystalline sizes can slower the agglomeration process. Yeh et al. reported that a wide size distribution of particle size slows significantly the sintering process at high temperature [52].

A smaller crystallite size for $CeVO_4$ phase was observed on 11Ce-CeV solid after synthesis and after thermal aging at 600°C whereas a smaller crystallite size was observed on 13Ce-CeV solid after thermal aging at 850°C. This evolution is in line with the highest NOx conversion of 11Ce-CeV after thermal aging at 600°C and the highest NOx conversion of 13Ce-CeV after thermal aging at 850°C in Fast-SCR conditions.

The coexistence of CeO_2 was found as a key parameter for samples with cooperative effects on the NO_x conversion to nitrogen regardless of the operating conditions. The formation of more reducible VO_x species at the surface is also consistent with H_2-TPR. In this sense, H_2-TPR measurements highlight that 11Ce-CeV and 13Ce-CeV catalysts have better redox properties than that of Ce-CeV catalyst. The higher Ce^{4+}/Ce^{3+} ratio may result in the higher SCR activity due to the intensified oxygen storage between Ce^{4+} and Ce^{3+} via the following equations $2CeO_2 \rightarrow Ce_2O_3 + O^*$ and $Ce_2O_3 + 1/2\ O_2 \rightarrow 2CeO_2$, which can promote the oxidation of NO to NO_2 [5]. Therefore, the NO oxidation to NO_2 occurs as suggested [53]:

$NO\ (g) \rightarrow NO\ (a)$

$2CeO_2 \rightarrow Ce_2O_3 + O^*$

$NO\ (a) + O^* \rightarrow NO_2\ (a)$

$Ce_2O_3 + 1/2O_2 \rightarrow 2CeO_2$

As listed in Table 2, the evolution of the Ce^{4+}/Ce^{3+} ratio consistently with O_α/O_β ratio is in good agreement with the previous statement.

The role of Lewis and Bronsted acid sites is mainly discussed on $V_2O_5/WO_3/TiO_2$ catalyst in the literature. Topsoe et al. propose that Brønsted acid sites are the main active sites in NH_3-SCR [54]. On the other hand, Ramis et al. report that Lewis acid sites coordinate more strongly NH_3 than Brønsted acid sites with respect to temperature [55]. Marberger et al. observe a faster consumption of ammonia adsorbed on Lewis acid sites than of ammonia adsorbed on Brønsted acid sites after introduction of NO in lean condition. They state that Bronsted acid sites act as an NH_3 reservoir and that the active sites consist on mono-oxo vanadyl groups (Lewis acid sites) [56]. Pyridine adsorption on Ce-CeV aged at 600°C underlines the very low concentration of Lewis acid sites (1.3 µmol/g) associated to the low specific surface area (6 m^2/g) (Fig. S6 and Table S2). The number of Lewis acid sites increases on 11Ce-CeV and 13Ce-CeV solids but still remains limited.

Peng et al. proposed that CeO_2 creates the new Lewis acid sites and $CeVO_4$ could form Brønsted acid sites [57]. The formation of Brønsted acid sites on Ce-CeV solid is not observed in our conditions. They concluded that at 150 and 250°C the cis-$(N_2O)_2^{2-}$ and $(NO)_2$ species are responsible for the activity, these species react with the adsorbed NH_3 species (Lewis and Brønsted acid sites). At high temperature (350°C), the nitrate and nitrite species can be involved in the reaction mechanism [57].

4 Conclusions

This study was devoted to the catalytic properties of bulk $CeVO_4$ solids with excess CeO_2 (11 and 13 wt.%) prepared by hydrothermal synthesis and further aged at 600°C or 850°C in the presence of steam. The physicochemical properties were studied using ICP, XRD, Raman, BET, H_2-TPR and XPS analysis before and after aging. The XRD patterns put into evidence the coexistence of the zircon-type

structure of $CeVO_4$ and the segregation of CeO_2 after aging at 600°C and Ce_7O_{12} after aging at 850°C. It is worthy to mention that the loss of vanadium in the elemental analysis was not observed after aging, which suggested the strong stabilization of V^{5+} species in $CeVO_4$ structure. High specific surface area (up to 102 m^2/g) was obtained for solid with 11 wt % of CeO_2 in excess. The presence of segregated ceria was found to promote the catalytic performances of the catalyst. The best catalytic performances were obtained on 11Ce-CeV with the selective conversion of NO_x into nitrogen between 250 and 450°C after thermal aging at 600°C. The change of oxidation properties led to the promotion of NH_3 oxidation when CeO_2 content reached 13 wt.%. Such enhancement could be related to an increased density of sites provided by CeO_2 for oxidizing NO to NO_2 which ensures a faster re-oxidation of V (IV) to V (V) compared to O_2 in standard conditions.

Acknowledgments

The FEDER, the CNRS, the Région Nord Pas-de-Calais and the Ministère de l'Education Nationale de l'Enseignement Supérieur et de la Recherche are acknowledged for fundings of XPS/LEIS/ToF-SIMS spectrometers within the Pôle Régional d'Analyses de Surface and X-ray diffractometers. The authors would like to thank Olivier Gardoll (UCCS), Laurence Burylo (UCCS), Pardis Simon and Martine Trentesaux (UCCS) for conducting the H_2-TPR, XRD and XPS measurements respectively.

References

[1] Ogidiama OV. and Shamim T (2014) Energy Procedia 61:2154–2157
[2] Zhang HL, Zhu Y, Wang SD, Zhao M, Gong MC, and Chen YQ (2015) Fuel Process. Technol 137(2):38–47
[3] Liu S, Wu X, Weng D, Li M and Lee HR (2012) Chem. Eng. J. 203:25–35
[4] Millo F, Rafigh M, Fino D and Miceli P (2017) Fuel 198:183–192
[5] Gao F, Tang X, Yi H, Zhao S, Li C, Li J, Shi Y and Meng X (2017) Catalysts 7(7):199-231
[6] Xie X, Lu J, Hums E, Huang Q and Lu Z (2015) Energy Fuels 29(6):3890–3896
[7] Zhang Q, Song C, Lv G, Bin F, Pang H and Song J (2014) J. Ind. Eng. Chem. 19(1):160–166
[8] Gruber M and Hermann K (2013) J. Chem. Phys. 138(9):094704
[9] Liu Q, Liu Z and Li C (2006) Chinese J. Catal. 27(7):636–646
[10] Yao X, Zhao R, Chen L, Du J, Tao C, Yang F and Dong L (2017) Appl. Catal. B Environ. 208:82–93
[11] Moreau P, Valero P, Tschamber V, Brillard A, Brilhac JF, Hohl Y and Vonarb R (2015) SAE Technical Papers 2015-24-2503:1–6,.
[12] Lian Z, Liu F and He H (2015) Catal. Sci. Technol. 5(1):389–396

[13] Peng Y, Li J, Chen L, Chen J, Han J, Zhang H and Han W (2012) Environ. Sci. Technol. 46(5):2864–2869
[14] Wang X, Shi A, Duan Y, Wang J and Shen M (2012) Catal. Sci. Technol. 2(7): 1386-1395
[15] Xu L, Li XS, Crocker M, Zhang ZS, Zhu AM and Shi C (2013) J. Mol. Catal. A Chem. 378(2):82–90
[16] Krishna K, Seijger GBF, Van Den Bleek CM and Calis HPA (2002) Chem Comm, 2(2):2030–2031
[17] Tang C, Zhang H and Dong L (2016) Catal. Sci. Technol. 6(5):1248–1264
[18] Shan W, Liu F, Yu Y and He H (2014) Cuihua Xuebao/Chinese J. Catal. 35(8):1251–1259
[19] Qi G, Yang RT and Chang R (2004) Appl. Catal. B Environ. 51(2):93–106
[20] Zhao X, Huang L, Li H, Hu H, Hu X, Shi L and Zhang D (2016) Appl. Catal. B Environ. 183:269–281
[21] Shen Y, Zhu S, Qiu T and Shen S (2009) Catal. Commun. 11(1):20–23
[22] Gao X, Jiang Y, Fu Y, Zhong Y, Luo Z and Cen K (2010) Catal. Commun. 11(5):465–469
[23] Adamowska M, Krztoń A, Najbar M, Da Costa P and Djéga-Mariadassou G (2008) Catal. Today 137:288–291
[24] Zeng Y, Zhang S, Wang Y and Zhong Q (2017) J. Colloid Interface Sci. 496:487–495
[25] Khan MN, Han L, Wang P, He J, Yang B, Yan T, Shi L, Zhang D (2020) Chem. Eng. J. 397:125535
[26] Yu J, Si Z, Zhu M, Wu X, Chen L, Weng D and Zou J (2015) RSC Adv. 5:83594–83599
[27] Qi G and Yang RT (2003) J. Catal. 217(2):434–441
[28] Wang D, Jangjou Y, Liu Y, Sharma MK, Luo J, Li J, Kamasamudram K and Epling WS (2015) Appl. Catal. B Environ. 165:438–445
[29] Valdez Lancinha Pereira M, Nicolle A and Berthout D (2015) Catal. Today 258:424–431
[30] Gillot S, Tricot G, Vezin H, Dacquin JP, Dujardin C and Granger P (2017) Appl. Catal. B Environ. 218(2):338–348
[31] Casanova M, Schermanz K, Llorca J and Trovarelli A (2012) Catal. Today 184(1):227–236
[32] Casanova M, Llorca J, Sagar A, Schermanz K and Trovarelli A (2015) Catal. Today 241:159–168
[33] Bellakki MB, Baidya T, Shivakumara C, Vasanthacharya NY, Hegde MS and Madras G (2008) Appl. Catal. B Environ. 84(3–4):474–481
[34] Gillot S, Dacquin JP, Dujardin C and Granger P (2016) Top. Catal. 59(10–12):987–995
[35] Ayodhya AS, Lamani VT, Thirumoorthy M and Kumar GN (2019) J. Energy Inst. 92(2):341-350
[36] Tuenter G, van Leeuwen WF and Snepvangers LJM (1986) Ind. Eng. Chem. - Prod. Res. Dev. 25(4):633–636
[37] Kato A, Matsuda S, Kamo T, Nakajima F, Kuroda H and Narita T (1981) J. Phys. Chem. 85(26):4099–4102
[38] Zhang L, Pierce J, Leung VL, Wang D and Epling WS (2013) J. Phys. Chem. C 117:8282–8289
[39] Tang C, Zhang H and Dong L (2016) Catal. Sci. Technol.6:1248–1264
[40] Koebel M, Madia G, Raimondi F and Wokaun A (2002) J. Catal. 209:159-165
[41] Dumesic JA, Topsøe NY, Topsøe H, Chen Y, Slabiak T (1996) J. Catal. 163(2):409-417
[42] Chen L (2006) Mater. Lett. 60(15):1859–1862
[43] Shoko E, Smith MF and McKenzie RH (2010) J. Phys. Condens. Matter 22:223201-223218
[44] Agula B, Ren T, Zhao X, Zhaorigetu B and Yuan Z (2011) J. Natural. Gas Chem. 20(3):232–236
[45] Shen M, Xu L, Wang J, Li C, Wang W, Wang J and Zhai Y (2016) J. Rare Earths 34(3):259–267
[46] Yang H, Zha J, Zhang P, Qin Y, Chen T and Ye F (2017) Sensors Actuators, B Chem. 247:469-478
[47] Anandan C and Bera P (2015) Surf. Interface Anal. 47(7):777–784
[48] Romeo M, Bak K, El Fallah J, Le Normand F and Hilaire L (1993) Surf. Int. Anal. 20:508-512
[49] Liu L, Shi J, Cao H, Wang R and Liu Z (2017) Beilstein J. Nanotechnol. 8:2425–2437
[50] Huang H, Gu Y, Zhao J and Wang X (2015) J. Catal. 326(3):54–68
[51] Światowska-Mrowiecka J, Maurice V, Zanna S, Klein L and Marcus P (2007) Electrochim. Acta 52(18):5644–5653
[52] Yeh TS, Sacks MD (1990) Ceramic Trans. 7:309-331
[53] Chang H, Chen X, Li J, Ma L, Wang C, Liu C, Schwank JW and Hao J (2013) Environ. Sci. Technol. 47(10):5294–5301
[54] Topsoe NY (1994) Science 265:1217-1219
[55] Ramis G, Busca G, Bregani, F, Forzatti P (1990) Appl. Catal. 64:259-27

[56] Marberger A, Ferri D, Elsener M, Krocher O (2016) Angew. Chem., Int. Ed. 55:11989-11994
[57] Peng Y, Wang C and Li J (2014) Appl. Catal. B Environ. 144:538–546